Segmentation of the Liver Using the Deformable Contour Method on CT Images

Seong-Jae Lim[1], Yong-Yeon Jeong[2], and Yo-Sung Ho[1]

[1] Gwangju Institute of Science and Technology (GIST),
1 Oryong-dong, Buk-gu, Gwangju 500-712, Korea
{sjlim, hoyo}@gist.ac.kr
[2] Chonnam National University Medical School,
8 Hack-dong, Dong-gu, Gwangju 501-757, Korea

Abstract. Automatic liver segmentation from abdominal computed tomography (CT) images is one of the most important steps for computer-aided diagnosis (CAD) for liver CT. However, the liver must be separated manually or semi-automatically since surface features of the liver and partial-volume effects make automatic discrimination from other adjacent organs or tissues very difficult. In this paper, we present an unsupervised liver segmentation algorithm with three steps. In the preprocessing, we simplify the input CT image by estimating the liver position using a prior knowledge about the location of the liver and by performing multilevel threshold on the estimated liver position. The proposed scheme utilizes the multiscale morphological filter recursively with region-labeling and clustering to detect the search range for deformable contouring. Most of the liver contours are positioned within the search range. In order to perform an accurate segmentation, we produce the gradient-label map, which represents the gradient magnitude in the search range. The proposed algorithm performed deformable contouring on the gradient-label map by using regular patterns of the liver boundary. Experimental results are comparable to those of manual tracing by radiological doctors and shown to be efficient.

Keywords: Liver segmentation, Morphological filtering, Deformable contouring, Computer-Aided Diagnosis(CAD).

1 Introduction

Liver cancer is one of the most common internal malignancies worldwide. The hepatocelluar carcinoma is common in Asia and metastasis is common in the West. Computed tomography (CT) has been identified as accurate noninvasive imaging modalities in the diagnosis of the liver cancer. Designing and developing computer-assisted image processing techniques to help doctors improve their diagnosis has received considerable interests over the past years [1]. CT images are interpreted by radiologists. However, image interpretation by human beings is often limited due to the non-systematic search patterns of themselves, the presence of structural noise in the image, and the presentation of complex disease states requiring the integration of a vast amount of image data and clinical information.

Y.-S. Ho and H.J. Kim (Eds.): PCM 2005, Part I, LNCS 3767, pp. 570–581, 2005.

Recently, the computer-aided diagnosis (CAD), defined as a diagnosis introduced by a radiologist who uses the output from a computerized analysis of medical images as a "second opinion" in detecting lesions, assessing extent of disease, and making diagnostic decisions, is being used to improve the interpretation components of medical imaging [2],[3]. Considerable and serious efforts have been made toward the development of CAD systems in diagnostic radiology.

However, CAD research for liver against mammogram and chest radiographs is to be insufficient because the liver segmentation that plays an important role for CAD is difficult. This is mainly due to the following two facts. The first one is the proximity of the liver and other organs or muscles having similar intensity values. It makes resolution difficult by observation of intensity discontinuity alone because of the partial-volume effects (PVE), i.e., the mixing of different tissue types in a single voxel. PVE causes edge blurring between different tissue types and reduces the accuracy and reliability of measurements taken on the image. The second one is the shape variation across patients even on the same patient [4].

For image segmentation, there are various approaches, such as feature thresholding, contour-based methods, region-based methods, clustering, and template matching [5]. Each of these approaches has its advantages and disadvantages in terms of applicability, suitability, performance, and computational cost. Particularly, any approaches cannot guarantee desirable results on liver segmentation without considering characteristics of the abdominal CT image.

In this paper, we propose an automatic liver segmentation algorithm in abdominal CT images, which is a combination of region-based and contour-based approaches. Our algorithm exploits multiscale morphological filtering and the deformable contour method using labeling-based search algorithm to address these problems. In order to increase the robustness of the method, we use an estimated liver position (ELP), which is composed of control points and fitted into the patient map. ELP enables us to find robust patient contour and is used to perform proper liver segmentation [6].

2 Segmentation of the Liver

Mainly, the liver is approximated to muscle and gastrointestinal tract. Since adjacent organs have similar intensity values as the liver, a direct liver-extraction approach may extract undesirable boundaries resulting from its adjacent organs as fault positive/negative errors [1]. In order to cope with the problem, we present a new segmentation scheme, consisting of three stages: image simplification as preprocessing, search range detection using multiscale morphological filtering, and contour-based segmentation using the labeling-based search algorithm.

2.1 Image Simplification

For image simplification, we consider a prior knowledge of the liver on the abdominal CT image, such as shape, location, and intensity value.

Estimated Liver Position (ELP). For histogram considering only pixels within the patient contour, we introduce the ELP. In order to find the ELP, we use prior knowledge, such as a general location, shape and attenuation of the liver. An abdominal CT image typically consists of six components: background/air, liver, soft tissue, bone/vessel, kidney, and gastrointestinal tract. The liver is generally located in the left side of abdominal CT images and existed within the ribs [2]. We use the fact that the liver is positioned within the ribs. Since the attenuation of the ribs is almost white gray-level like the bone, we can easily detect the ribs. Figure 1 shows the estimation result of the liver position.

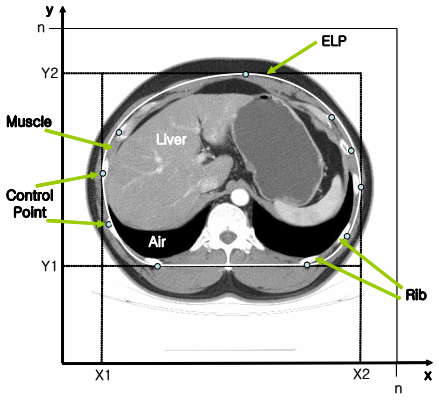

Fig. 1. Estimation of Liver Position

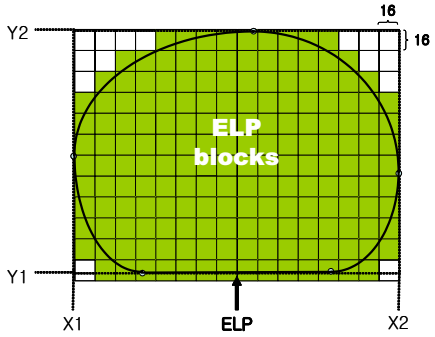

Fig. 2. ELP Blocks

In Fig. 1, the four patient extensions $(X1, X2, Y1, Y2)$ in the x and y direction are calculated by finding control points. Those control points are determined by the outmost point of each rib. Finally, the ELP becomes the spline curve connecting all of the control points, as shown Fig. 1. The liver is always located with in the ELP. For more accurate and simple processing, we make the ELP blocks, which are 16x16 blocks including the ELP, as shown in Fig. 2.

Histogram Analysis. We analyzed the intensity distribution of about 20 number of CT samples that are manually segmented liver and adjacent muscle, as shown in Fig. 3. In addition, we interpret Hounsfield numbers correspond to the liver and muscle into the gray level. Finally, we found that the intensity distribution of the liver is similar to the Gaussian distribution. In Fig. 3, however, attenuation of the liver and muscle is overlapped on some places. Hence, we estimate a threshold δ from the overlapped location to divide two objects. Assuming a Gaussian distribution with mean μ and standard deviation σ, the probability $P\{x; |x - \mu| \leq 2\sigma\} \simeq 95\%$, we can propose to set δ equal to 2σ [7].

Since the distribution function is similar to the normal distributed Gaussian function, as shown in Fig. 3, we estimate the mean μ_l for the liver and μ_m for

the muscle by finding peaks in the intensity distribution of the ELP. We then obtain the standard deviation σ_l for the liver and σ_m for the muscle by fitting the gaussian density function on the intensity distribution function. Finally, we decide the threshold value δ_l for the liver and δ_m for the muscle. Thus, the ELP is classified into three classes by using the threshold value: liver class($\mu_m + \delta_m < C \leq \mu_l + \delta_l$), chaos class($\mu_l - \delta_l < C \leq \mu_m + \delta_m$), and non-liver class(others), where C is the class. Multilevel thresholding based on the analysis of the intensity distribution makes many other organs or tissues disappear in ELP blocks and identifies the liver and adjacent region as clear or blurred liver region.

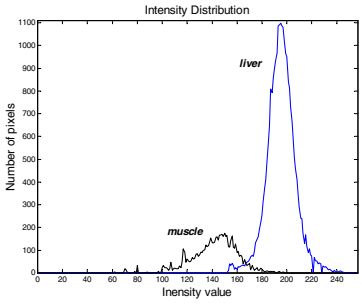

Fig. 3. Histogram of Several CT Samples

2.2 Search Range Detection

We find the first and second search region by performing multiscale morphological operations on the threshold image of the image simplification for the precise liver boundary.

Multiscale Morphological Filtering. Preprocessing classifies each pixel into the clustered liver class and the scattered non-liver class. Accordingly, we perform mathematical morphology filtering to reduce the scattered class and detect the liver object. This set theoretic, shape oriented approach treats the image as a set and the kernel of operation as another set, commonly known as structuring element. Different standard morphological operations, namely erosion, dilation, opening, and closing, are basically set theoretic operations between these two sets. The shape and the size of the structuring element play an important role in detecting or extracting features of the given shape and size from the image [5].

In constructing a morphological filter, we use erosion and dilation with a flat structuring element as follows [8], [9],

$$(f \ominus B_n)(x, y) = min\{f(x + l, y + m)|(l, m) \in B_n\} \tag{1}$$

$$(f \oplus B_n)(x, y) = max\{f(x - l, y - m)|(l, m) \in B_n\}. \tag{2}$$

Though the structuring element B takes care of the shape of the features during processing the image, it cannot equally treat the objects of the same shape but of the different size. Thus, for processing objects based on their shape as well as size, we incorporate a second attribute to the structuring element: its scale or composition. The types of morphological operations are termed as multiscale morphology [10]. Multiscale filtering are defined by

$$(f \ominus kB_n)(x,y) = \{(((f \ominus \underbrace{B_n) \ominus B_n) \cdots \ominus B_n}_{k \text{ times}})(x,y)\} \tag{3}$$

$$(f \oplus kB_n)(x,y) = \{(((f \oplus \underbrace{B_n) \oplus B_n) \cdots \oplus B_n}_{k \text{ times}})(x,y)\} \tag{4}$$

where k is an integer representing the scale factor of the structuring element B and n is the size of B. Multiscale filtering is performed by using the composition of the kth order morphological erosion and dilation operations with the multisize structuring elements of the 5x5 and 3x3 flat size. The size of structuring elements is decided by analyzing the number of remained regions or pixels of the threshold image, and the k value is experimentally set to 4 or 5.

First Search Range Detection. For the detection of the first search region, firstly, we find the initial liver region by performing multiscale opening. In multiscale opening, the erosion operation of k times, as its first step, eliminates bright features that do not fit within the structuring element and unconnected and scattered features in the threshold image. Then, it dilates iteratively same times to the erosion operation to restore the contours of components that have not been completely removed by the first step [2].

In the second stage, multiscale filtering using the fixed order of filtering composition causes dispersed pixels of tissues. It is due to the various shape or size of the liver by patients. In order to solve this problem, we perform on the 4-connected region-labeling algorithm based on the breadth-first search approach [11]. After the performance of the region-labeling algorithm, the largest labeled region is marked out for the coarse liver region.

The labeled liver region still has noise, such as adjoining muscles. Thus, we classify the labeled image into three classes by using the modified K-means algorithm. The adjacent tissues or muscles to the liver mainly have a higher or lower intensity value than that of the liver. Therefore, we use three centroids for the modified K-means algorithm that the middle centroid corresponding to the mean value of the liver is just computed again and the others are fixed to the max and min intensity value in the labeled liver region. This processing divides the region into the adjacent noise which will be reduced and the initial liver region.

The first search region is constructed by performing the different order's composition between erosion and dilation operations of the mathematical morphological opening on the clustered initial liver region by

$$(f \circ iB_n)(x,y) = ((f \ominus iB_n) \oplus (i+j)B_n)(x,y) \tag{5}$$

where i is the scale factor of the structuring element and j is a parameter which decides the size of search range. Generally, i is set to 2 and j is 4 or 5.

Second Search Range Detection. In the clustering, instead of reducing the adjacent noise, any liver region can be reduced. In order to address this problem, reverse filtering of the first morphological filtering is performed on the region of the original image corresponding to the previous labeled region. Multiscale morphological closing recovers some regions of the liver which are damaged or reduced in the previous morphological opening. The second search region is constructed based on the result of the morphological closing, region-labeling, and modified K-means clustering similar to the previous processing.

Multiscale morphological closing is defined, respectively, by

$$(f \bullet iB_n)(x, y) = ((f \oplus iB_n) \ominus (i + j)B_n)(x, y) \tag{6}$$

The final search range is determined by excluding the second search region from the first search region. Since most of the liver boundaries are located in this search range, precise automatic liver segmentation is possible by using the deformable contour algorithm within this range. Furthermore, the initial liver boundary which will be a guidepost for the search algorithm constructed by extension of the second search region to the original liver size.

2.3 Contour-Based Liver Segmentation

The initial liver boundary acquired by morphological filtering is a coarse liver contour. Therefore, we present the labeling-based search algorithm that deforms the initial liver boundary within the search range to find clear and final liver contour. For the search algorithm, we make a gradient-label map.

Gradient-Label Map. Since the slice thickness of our CT data set is 5mm, PVE is occurred at the boundary of the adjacent object. Because occurrences of PVE yield a gradual intensity fall across the boundaries of objects, a labeling-based search algorithm with an intensity partition that is sufficiently fine results in labeled images whose isolabel contours form conspicuous patterns. Because isolabel-contour patterns resemble isoelevation contours on topographical maps, we refer to the labeled images as isolabel-contour maps. If we observe an area within an isolabel-contour map that extends from one object's center to its boundary within the search range, we see a distinct pattern. Where the intensity gradient is monotonic in the raw image, the pattern of labels in the isolabel-contour map is monotonic as well. We observe dense contour patterns in the areas of abrupt intensity gradients and widespread contour patterns in the areas of gradual intensity gradients [4]. In order to make a gradient-label map, we enhance the isolabel-contour map by using the gradient magnitude into the weighing factor.

The spatial gradient of the search range image is approximated by using of a morphological gradient operator, expressed by

$$G(f) = \{(f \oplus B_n)(x, y) - (f \ominus B_n)(x, y)\} \tag{7}$$

The gradient image usually indicating borders between neighbor regions within search range is weighted by being reversed and normalized.

Labeling-Based Search Algorithm. We can describe the entire patterns of liver contours by classifying into three patterns in a gradient-label map as a relationship of the intensity distribution.

- Pattern 1: The liver is adjacent to the air region which has low intensity value.
- Pattern 2: The liver is touched to the ribs or the kidney which has high intensity value.
- Pattern 3: The liver is adjoined to the stomach, the intensity value within the liver boundary is distributed through the low gray-level.

The deformable contouring is started from the lowest located pixel of the initial liver contour toward the clockwise direction on the gradient-label map. Fig. 4 shows the eight directions which the current pixel can proceed. Liver boundary is smooth since the liver is the human organ. Therefore, the directions that the current pixel can proceed are three directions indicated by the small arrows in Fig. 4. Among the three directions, the center direction is determined by the initial liver contour obtained in the second stage. If the current pixel is located on the initial liver contour, then the next direction is determined by the initial liver contour. Otherwise, the next direction is the same as the previous direction. The other two possible directions are on either side of the center direction, as shown in Fig. 4. All of three directions are the candidate pixels.

Arrows indicate pixels considered for cost function within 9x9 window.

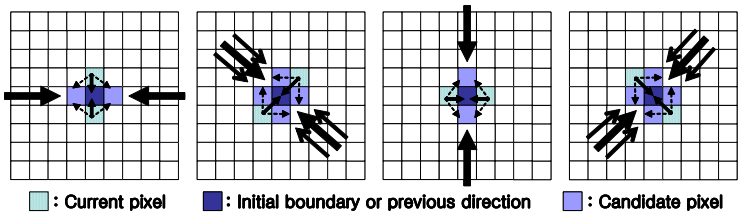

Fig. 4. Search Map

For the optimal path from each pixel, we formulate the local cost function at each candidate pixel. We can get a correct liver contour by finding optimal path which is the minimal cost value. The local cost function combining three features is defined as,

$$l(p,q) = w_D \cdot f_D(p,q) + w_B \cdot f_B(q) + w_I \cdot f_I(q) \tag{8}$$

where each w is the weight of the corresponding feature function. The p and q are two neighboring pixels in the gradient-label map, and $l(p,q)$ represents the local

cost on the directed link from p to q and the two pixel value components, f_B and f_I, are "initial boundary" and "intensity distribution" cost functions. [12].

The f_D is a function of gradient direction which adds smoothness constraint to the boundary by associating a relatively high cost for sharp changes in boundary direction. The gradient direction feature cost is

$$f_D(p,q) = \frac{2}{3\pi}\{acos[d_p(p,q)] + acos[d_q(p,q)]\} \tag{9}$$

where $D'(p)$ is the unit vector perpendicular to the gradient direction at a point p. In addition, $d_p(p,q) = D'(p) \cdot L(p,q)$ and $d_q(p,q) = L(p,q) \cdot D'(q)$ are vector dot products and $L(p,q)$ is the normalized bidirectional link or the unit edge vector between pixels p and q and simply computes the direction of the link between p and q so that the difference between p and the direction of the link is minimized [12].

One of the two pixel components, $f_B(q)$ is the function estimating the state of the candidate pixel about the initial boundary. The state is inside or outside position in the gradient-label map. For the pixel component of the intensity distribution, we formulate the cost function, $f_I(q)$, by following the search map, as shown in Fig. 4. Functions $f_B(q)$ and $f_I(q)$ are

$$f_B(q) = \frac{1}{255}\{I(q) \cdot s\} \qquad and \qquad f_I(q) = \frac{1}{255}\{I(q) \cdot P(n)\} \tag{10}$$

where $I(q)$ is the pixel value at q and s is the weight of the state. If pixel is "inside" and "outside", s is 0.4. Otherwise, s is 0.2. $P(n)$ indicates a kind of the pattern as mentioned above. Each pattern is decided by searching neighboring pixels of each candidate pixel on bidirectional large arrows within the 9x9 window, as shown in Fig. 4. If the current pixel goes to the perpendicular direction, then the neighboring eight pixels of the candidate pixel that correspond to the initial boundary or previous direction are examined whether those are on the above pattern. The neighboring pixels within 9x9 window of the other candidate pixels are also examined. $P(n)$ value is experimentally determined but if the candidate pixel satisfies the pattern, $P(n)$ can generally take a value from 0.2 to 0.4. Otherwise, $P(n)$ is set to 1.

3 Experimental Results and Analysis

We experimented several samples with various shapes and irregular texture of 10 patients. All of the samples are contrast-enhanced abdominal CT images of venous phase.

Fig. 5 shows the results of each process of the proposed algorithm. Fig. 5(a) shows the original CT image. Fig. 5(b) depicts the multilevel threshold image on ELP blocks. We simplified the CT image using multilevel thresholding, which is decided by considering the feature of the gaussian distribution. It is due to the intensity distribution of the liver which is similar to the gaussian distribution. We can see that many other organs and tissues are eliminated in the threshold image.

However, unconnected or small tissues are remained. In order to reduce these objects and preserve the liver region, we perform recursively multiscale morphological filtering with region-labeling and clustering, as shown in Fig. 5(c) and Fig. 5(d). The appropriate composition of the order of morphological operations with region-labeling and clustering makes the suitable search range for the liver contour as depicted in Fig. 5(c) and Fig. 5(d). Final search range is formed by subtracting the second search region from the first search region, as shown in Fig. 5(e). In addition, for deformable contouring, we construct the initial liver boundary by extension of the second search region to original liver size, as shown in Fig. 5(f).

Lastly, deformable contouring based on the labeling-based search algorithm finds the final liver contour in the search range. For deformable contouring we make the gradient-label map weighted by gradient magnitude on search range, as shown in Fig. 5(g). Final liver contour is determined by computing the minimum cost function considering the gradient direction, the intensity distribution and the pattern features of the liver, as shown in Fig. 5(h) and Fig. 6.

The results of the proposed algorithm were evaluated by comparing to results of manual tracing by radiologist. The exclusive-or method is used for the comparable measure. Table 1 shows the comparison of automatic and manual segmentation of the liver. The correctness average is about 96.8% and the error is about 3.2%. Fig. 5(h) and Fig. 6 show results of segmentation on the five patients. In addition to this, Table 1 presents results of the comparison of the area and error rate on the various locations in the abdominal CT of a patient.

Table 1. Comparison of automatic vs. manual segmentation of the liver (mm^2)

Sample	**Auto.**	**Manual**	**Error**(%)	**Sample**	**Auto.**	**Manual**	**Error**(%)
1	4493.17	4600.03	0.02320	9	9721.03	10085.35	0.03612
2	9492.12	9302.13	-0.02042	10	8225.13	7961.23	-0.03315
3	14498.81	14254.97	-0.01711	11	7510.97	6074.00	-0.02366
4	12832.21	12576.27	-0.02035	12	6321.27	6699.13	0.05640
5	12341.24	12688.73	0.02739	13	5006.03	5133.93	0.02491
6	13381.12	13017.53	-0.02793	14	4524.13	4675.53	0.03238
7	11194.59	11584.49	0.03366	15	3407.97	3536.56	0.03636
8	10320.27	10655.81	0.03149	16	3007.97	3056.56	0.01590

4 Conclusions

In this paper, we have proposed a new algorithm for automatic liver segmentation using a prior knowledge and the deformable contour method based on morphological filtering. We used the prior knowledge about the location of the liver in CT image and introduced the estimated liver position (ELP). Histogram analysis within the ELP is used to decide the adequate threshold value for multilevel thresholding that reduced computational complexity. In addition, multiscale morphological filtering using region-labeling and clustering detects the search

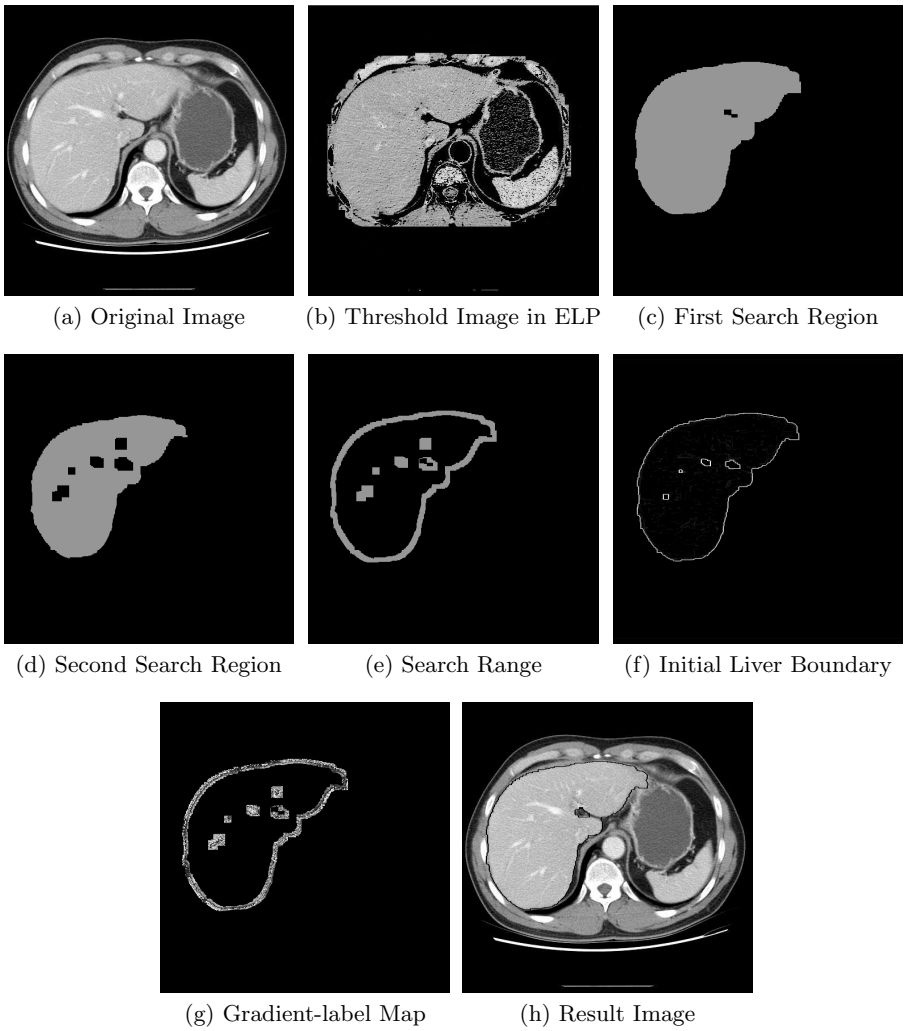

(a) Original Image (b) Threshold Image in ELP (c) First Search Region

(d) Second Search Region (e) Search Range (f) Initial Liver Boundary

(g) Gradient-label Map (h) Result Image

Fig. 5. Experimental Results of Patient 1

range and the initial liver boundary for the deformable contouring. The final contour is found by using the labeling-based search algorithm on the gradient-label map. The search algorithm considering partial-volume effect (PVE) computes the minimum cost function composed of the gradient magnitude, the gradient direction and the pattern of the intensity distribution. The final results are compared to manually segmented image by the radiologist, and we could know that the false positive/negative results were effectively suppressed. This algorithm is the effective automatic segmentation algorithm of the liver in CT images for the first step of the computer-aided diagnosis (CAD) and computer-aided surgery (CAS) systems. It will assist radiologists by improving their diagnosis.

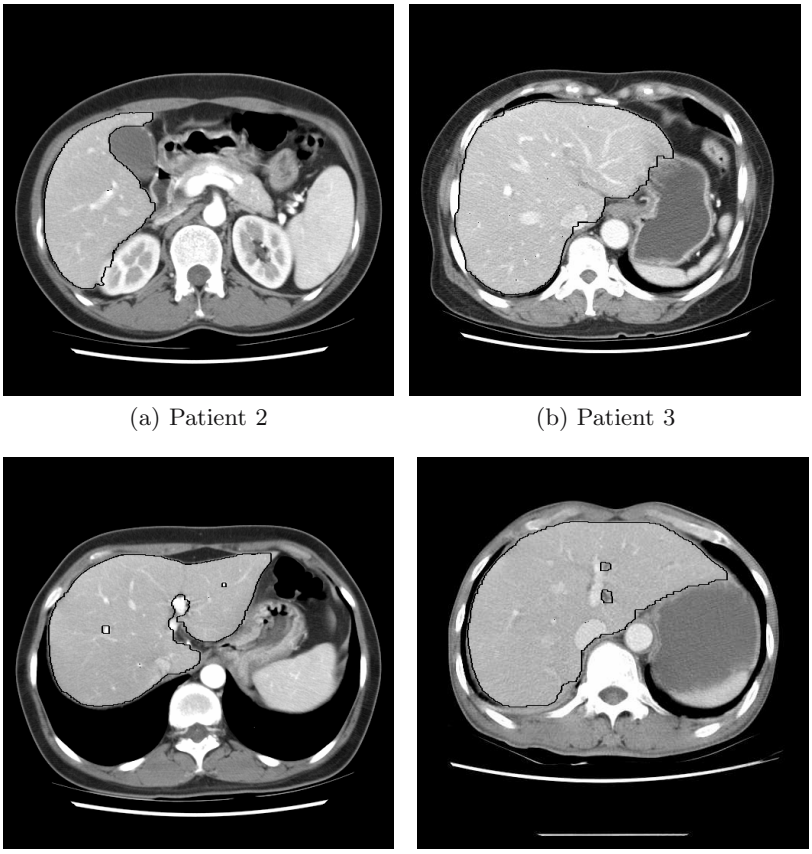

(a) Patient 2 (b) Patient 3

(c) Patient 4 (c) Patient 5

Fig. 6. Experimental Results

Acknowledgements. This work was supported by the Korea Research Foundation Grant (No. M07-2004-000-10140-0), in part by the Ministry of Information and Communication (MIC) through the Realistic Broadcasting Research Center (RBRC) at Gwangju Institute of Science and Technology (GIST), and in part by the Ministry of Education (MOE) through the Brain Korea 21 (BK21) project.

References

1. Chen, E.L., Chung, P.C., Chen, C.L., Tasi, H.M., Chang, C.I.: An Automatic Diagnosis System for CT Liver Image Classification. IEEE Transaction on Biomedical Engineering, Vol. 45, No. 6 (1998) 783-794
2. Lim, S.J., Jeong, Y.Y., Lee, C.W., Ho, Y.S.: Automatic Segmentation of the Liver in CT Images Using the Watershed Algorithm Based on Morphological Filtering. Proceeding of the SPIE, Vol. 5370 (2004) 1658-1666

3. Giger, M.L., Karssemeijer, N., Armato, S.G. III.: Guest Editorial : Computer-Aided Diagnosis in Medical Imaging, IEEE Transaction on Medical Imaging, Vol. 20, No. 12 (2001) 1205-1208
4. Shiffman, S., Rubin, G.D., Napel, S.: Medical Image Segmentation Using Analysis of Isolable-Contour Maps, IEEE Transaction on Medical Imaging, Vol. 19, No.11 (2000) 1064-1074
5. Mukhopadhyay, S., Chanda, B.: Multiscale Morphological Segmentation of Gray-Scale Images, IEEE Transaction on Image Processing, Vol. 12, No. 5 (2003) 533-549
6. Bilger, K., Kupferschlager, J., Muller-Schauenburg, W., Nusslin, F., Bares, R.: Threshold Calculation for Segmented Attenuation Correction in PET with Histogram Fitting, IEEE Transaction on Nuclear Science, Vol. 48, No. 1 (2001) 43-50
7. Kuo, C.H., Tewfik, A.H.: Multiscale Sigma Filter and Active Contour for Image Segmentation, Proceeding of the ICIP (1999) 353-357
8. Gonzalez, R.C., Woods, R.E.: Digital Image Processing, Prentice Hall (2002)
9. Kim, M.C., Choi, J.G., Kim, D.H., Lee, H., Lee, M.H., Ahn, C.T., Ho, Y.S.: A VOP Generation Tool: Automatic Segmentation of Moving Objects in Image Sequences Based on Spatio-Temporal Information, IEEE Transaction on Circuits and Systems for Video Technology, Vol. 9, No. 8 (1999) 1216-1226
10. Maragos, P.: Pattern Spectrum and Multiscale Shape Representation, IEEE Transaction on Pattern Analysis and Machine Intelligence, Vol. 11 (1989) 701-716
11. Gose, E., Johnsonbaugh, R., Jost, S.: Pattern Recognition and Image Analysis, Prentice Hall (1996)
12. Mortensen, E.N., Brrett, W.A.: Interactive Segmentation with Intelligent Scissors, Graphical Models and Image Processing, Vol. 60 (1998)